Journal Pre-proof

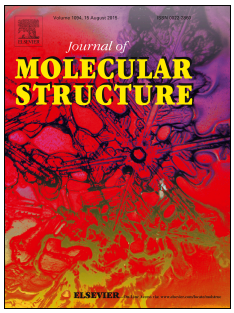

Design and application of (Fe_3O_4)-GO_{TfOH} based AgNPs doped starch/PEG-poly (acrylic acid) nanocomposite as the magnetic nanocatalyst and the wound dress

Shayan Forouzandehdel, Maryam Meskini, Mina Rezghi Rami

PII: S0022-2860(20)30467-1

DOI: https://doi.org/10.1016/j.molstruc.2020.128142

Reference: MOLSTR 128142

To appear in: *Journal of Molecular Structure*

Received Date: 9 February 2020

Revised Date: 15 March 2020

Accepted Date: 25 March 2020

Please cite this article as: S. Forouzandehdel, M. Meskini, M.R. Rami, Design and application of (Fe_3O_4)-GO_{TfOH} based AgNPs doped starch/PEG-poly (acrylic acid) nanocomposite as the magnetic nanocatalyst and the wound dress, *Journal of Molecular Structure* (2020), doi: https://doi.org/10.1016/j.molstruc.2020.128142.

Design and application of (Fe_3O_4)-GO_{TfOH} based AgNPs doped Starch/PEG-poly (acrylic acid) nanocomposite as the magnetic nanocatalyst and the wound dress

Shayan Forouzandehdel[a], Maryam Meskini[b], Mina Rezghi Rami[c]*

[a] Department of Chemistry, Sharif University of Technology, P. O. Box 11365-9516, Tehran, Iran
[b] Microbiology Research Center (MRC), Pasteur Institute of Iran, Tehran, Iran
[c] Department of Chemistry, K. N. Toosi University of Technology, P. O. Box 15875-4416, Tehran, Iran.

*rezghi@siptc.ir

Credit author statements:

Mina Rezghi Rami: Methodology, Conceptualization, Writing - Original Draft, Supervision, Project administration; **Shayan forouzandehdel**: Validation, Formal analysis, Resources, Funding acquisition; **Maryam Meskini**: Data Curation, Writing - Review & Editing, Visualization

Design and application of (Fe_3O_4)-GO_{TfOH} based AgNPs doped Starch/PEG-poly (acrylic acid) nanocomposite as the magnetic nanocatalyst and the wound dress

Shayan Forouzandehdel[a], Maryam Meskini[b], Mina Rezghi Rami[c]*

[a] Department of Chemistry, Sharif University of Technology, P. O. Box 11365-9516, Tehran, Iran
[b] Microbiology Research Center (MRC), Pasteur Institute of Iran, Tehran, Iran
[c] Department of Chemistry, K. N. Toosi University of Technology, P. O. Box 15875-4416, Tehran, Iran.

*rezghi@siptc.ir

Abstract: As a novel, recyclable nanocatalyst, (Fe_3O_4)-GO_{TfOH} based Ag nanoparticles doped Starch/PEG-poly (acrylic acid) nanocomposite (Fe_3O_4@GO_{TfOH}/Ag/St-PEG-AcA) was applied for one-pot synthesis of 2,4,6-triarylpyridine derivatives under water solvent conditions. The prepared nanocomposite was also evaluated in terms of biocompatibility for wound healing. Fe_3O_4@GO_{TfOH}/Ag/St-PEG-AcA could be easily removed from the mixture of the reaction by an external magnet and recycled without a considerable decrease of activity even after 10 runs. The new nanocatalyst offered better efficiencies than other commercially available sulfonic acid catalysts. In terms of the bioactivity of nanocatalyst, good antimicrobial efficiency was confirmed on *E. coli* bacteria. Besides, histology of repaired wounds in Fe_3O_4@GO_{TfOH}/Ag/St-PEG-AcA for a healed group of mice showed better fibroblast distribution and more compact collagen fiber organization compared to wounds in the control group.

Keywords: Magnetic nanocatalyst; Hydrogels; Wound healing; 2,4,6-triarylpyridines.

Introduction

On account of the most important and obvious advantages of heterogeneous catalysts such as easily separation and reusability for the production of fine chemicals[1] and increasing environmental concerns about liquid mineral acids[2], application of solid acids and development of efficient and recoverable heterogeneous catalysts has long been a goal in catalysis research[3].

It is renowned that graphene as a two-dimensional and one-atom-thick sheet of sp^2 bonded carbon atoms that are densely packed in a honeycomb crystal lattice and graphene oxide has been widely used in many different fields such as sensors[4], catalysis[5], adsorption[6], and energy storage[7]. Nano sheets of graphene oxide with high surface areas are covered by hydroxyl, epoxy, and

carboxylic groups which offer high water solubility for many applications. Graphene oxides contain a range of reactive oxygen functional groups, which offers it a good candidate for use in the mentioned applications through chemical functionalization [8]. Recently, GO-based poly(lactic acid) (PLA) stereo complex crystals (SCs) were designed by Xu et al. [9] to show elucidation of acceptable thermal and barrier properties, which may influence further extension of other material combinations. In the other study, Xu et al. [10] revealed that decrease the planar size of graphene oxide quantum dots (GOQDs), and the intercalation of functional groups containing oxygen, diminished the filler aggregation and improved the interfacial contacts with the host polymer. Their findings afforded intangible understandings of the significance of the dimensionality and surface chemistry of GO in the promising field of bionanocomposites.

Nanocomposite (NC) gels are considered due to their improved properties, for instance, the extraordinary mechanical property of organic-inorganic hybrid networks of nanocomposite gels[11]. Nano dispersions of metal nanoparticles are used to prepare nanocomposites due to their special properties, such as the large surface area to volume ratio and multiple applications[12]. Incorporation of silver nanoparticles (AgNPs) into the hydrogels has developed both mechanical properties and chemical stability of hydrogels, as well as increasing the adsorption capacity[13]. Besides, due to the antimicrobial properties of AgNPs, biocompatible polymers containing AgNPs have proven to be promising candidates for the biomedical area due to their superior antibacterial properties[14].

From a medical point of view, using NC for wound healing offers the possibility to absorb the exudate and reducing water evaporation to keep dehydration away. Preparing these conditions is considered an ideal environment for the wound healing process[15]. AgNPs and hydrogel-based biomaterials are non-cytotoxic and safe for patients in wound care management[16]. The unique intrinsic features of these materials promote wound healing and effectively control the growth of microorganisms at the wound site. This strategy plays an important role in the treatment of both acute and chronic wounds[17]. Recently, the development of AgNPs impregnated chitosan-poly ethylene glycol (PEG) hydrogel to accelerate wound healing in diabetic patients. The results illustrated a good porosity, high degree of swelling, and water vapor transition rate (WVTR) for AgNPs impregnated hydrogel as well as advanced antimicrobial and antioxidant properties *in-vitro* and enhanced wound healing capability *in-vivo* in diabetic rabbits[18]. Besides, stimuli-responsive chitosan (CS) and poly (N-vinyl-2-pyrrolidone) (PVP) have attained hydrogel properties in the presence of 74% neutralized polyacrylic acid (PAA). The biocompatibility of prepared hydrogel made them pertinent to drug delivery, and their release profile is examined

spectrophotometrically using silver sulfadiazine showed 91.2% of drug release in a consistent and controlled manner[19].

Over the past few years, the N-heterocyclic compounds, such as pyridines, are very helpful material for the development of molecules of pharmaceutical or biological interest[20]. Furthermore, conjugated molecules that have a pyridine core as the key unit, such as 2,4,6-triarylpyridines have also attracted much attention in previous years due to providing the impetus for further studies in utilizing this scaffold in new therapeutic drug classes[21, 22].

In our continuing efforts toward effective synthetic methodologies [23, 24], new environmental catalysts improvement, we aimed to formulate a new type of magnetically separable nanocomposite (Fe_3O_4)-GO_{TfOH} based AgNPs doped Starch/PEG-poly (acrylic acid) nanocomposite (Fe_3O_4@GO_{TfOH}/Ag/St-PEG-AcA) and its application for the synthesis of pyridine derivatives as well as a biocompatible nanocomposite as medication for wound healing. To the best of our knowledge, there has no such reported on the synthesis of a novel magnetic graphene-based bionanocomposite consist of starch, polyethylene glycol, acrylic acid, and AgNPs for simultaneous investigation of antimicrobial activities, promoting wound healing, and organic synthesis.

Experimental

Material

Acrylic acid (AcA; MW =72.06 g mol^{-1}, d= 1.06 g/cm^3) and ammonium persulfate (APS) were purchased from Fluka and used after vacuum distillation. N, N-methylene bis acrylamide (MBA) were purchased from Merck and used as received. Nanosilver liquid (20 nm, 99 %) was purchased from Mehregan Chemistry company. Soluble starch (Mw = 342.30), polyethylene glycol (PEG 4000, average mol wt 1,450 and d=1.0919 g/mL at 60 °C) and all other chemicals were purchased from Sigma-Aldrich. *Escherichia coli* (ATCC-25922) strain was kindly donated by the microbiology laboratory of Islamic Azad University, Tehran, Iran.

Preparation of Fe_3O_4@GO_{TfOH}

The GO dispersion was prepared using the Hummers method[25]. Then, the resulted GO is filtered and washed several times with ionized water. By coprecipitation and dispersion of 300 mg ferrous (Fe^{2+}) and 800mg ferric (Fe^{3+}) ions (50 ml) in the suspension of 40 mg GO and 40 ml H_2O under ultrasonication, Fe_3O_4@GO is achieved. Then, 2g trifluoromethanesulfonic acid was added to a suspension of Fe_3O_4@GO (1g) in 5ml CH_2CH_2, while mechanically stirred at 40ºC. The mixture

was filtered after 1 h, and the residue was washed with CH_2CH_2 and heated at 50 ^oC for 24 h under vacuum to obtained triflic acid-functionalized magnetic GO (**Figure 1**).

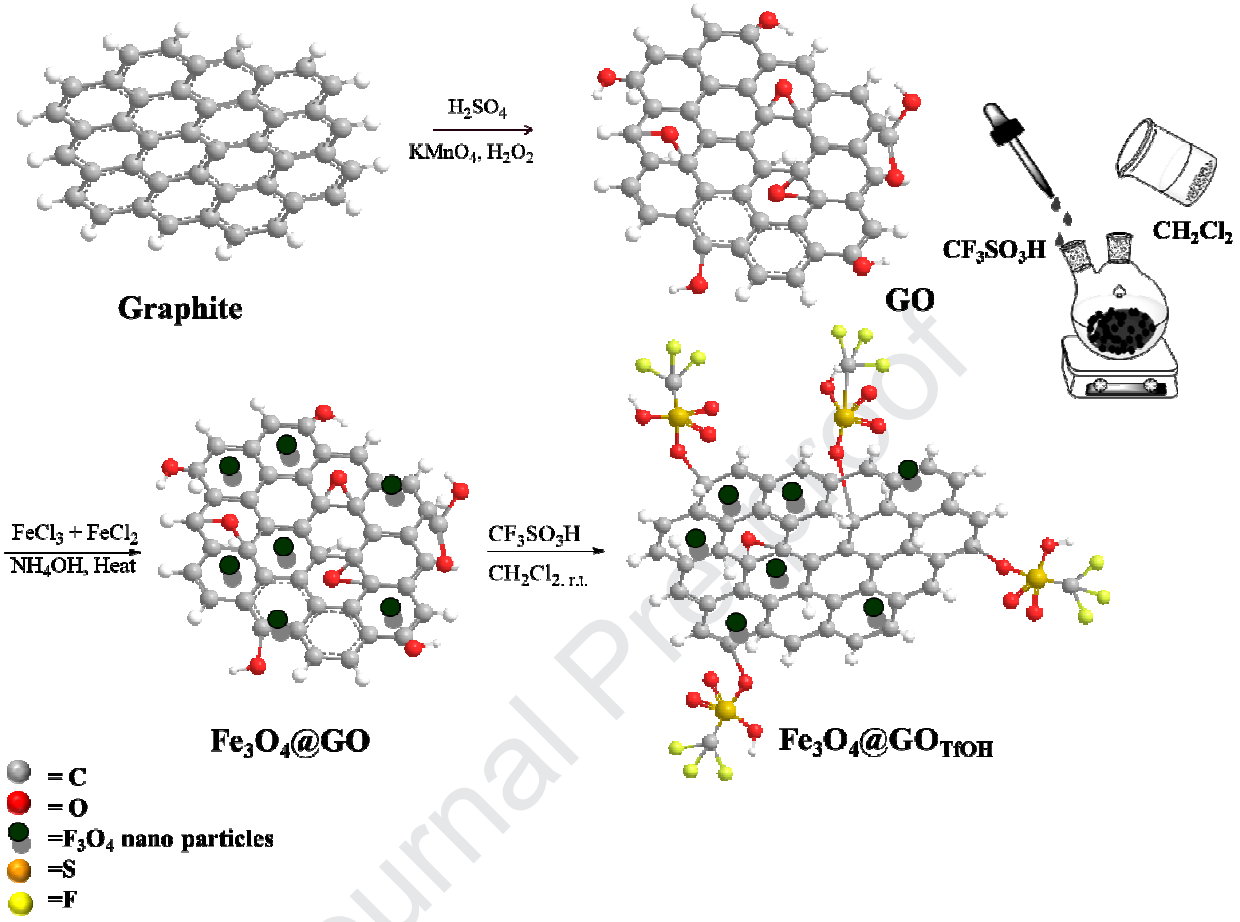

Figure 1: Synthesis of (Fe_3O_4)-GO-TfOH

Synthesis of Fe_3O_4@GO_{TfOH}/Ag/St-PEG-AcA

Briefly, starch (0.5 g) was solved in warm water at 80 °C. After 15 min, MBA (0.05 g) was dissolved in water (5 mL) and added to the aqueous solution with continuous mechanical stirring (300 rpm) until a homogeneous viscous mixture was obtained. The reaction temperature was controlled at 50 °C under an argon atmosphere, then a certain amount of 70 % neutralized AcA (6 mL), PEG (0.24 g) was added to the reaction mixture. At the next step, a definite amount of APS solution (0.08 g) was added into the mixture and was stirred for 10 min until the hydrogel was produced. After adding APS, the as-prepared AgNPs colloidal solutions (100-400ppm) and Fe_3O_4@GO_{TfOH} (0.5 g) were mixed with the above homogeneous solution and allowed to stir for 10 min. When the reaction was completed, the product was washed thoroughly with ethanol (100 mL)

to remove the unreacted materials (**Figure 2**). After filtering and drying of the samples, the viscosity of synthesized Fe_3O_4@GO_{TfOH}/Ag/St-PEG-AcA was determined using HVU 481viscometer (Herzog Contracting Corp-Germany Model) about 2.45 cP at 20 °C in order to investigate the size distribution of AgNPs.

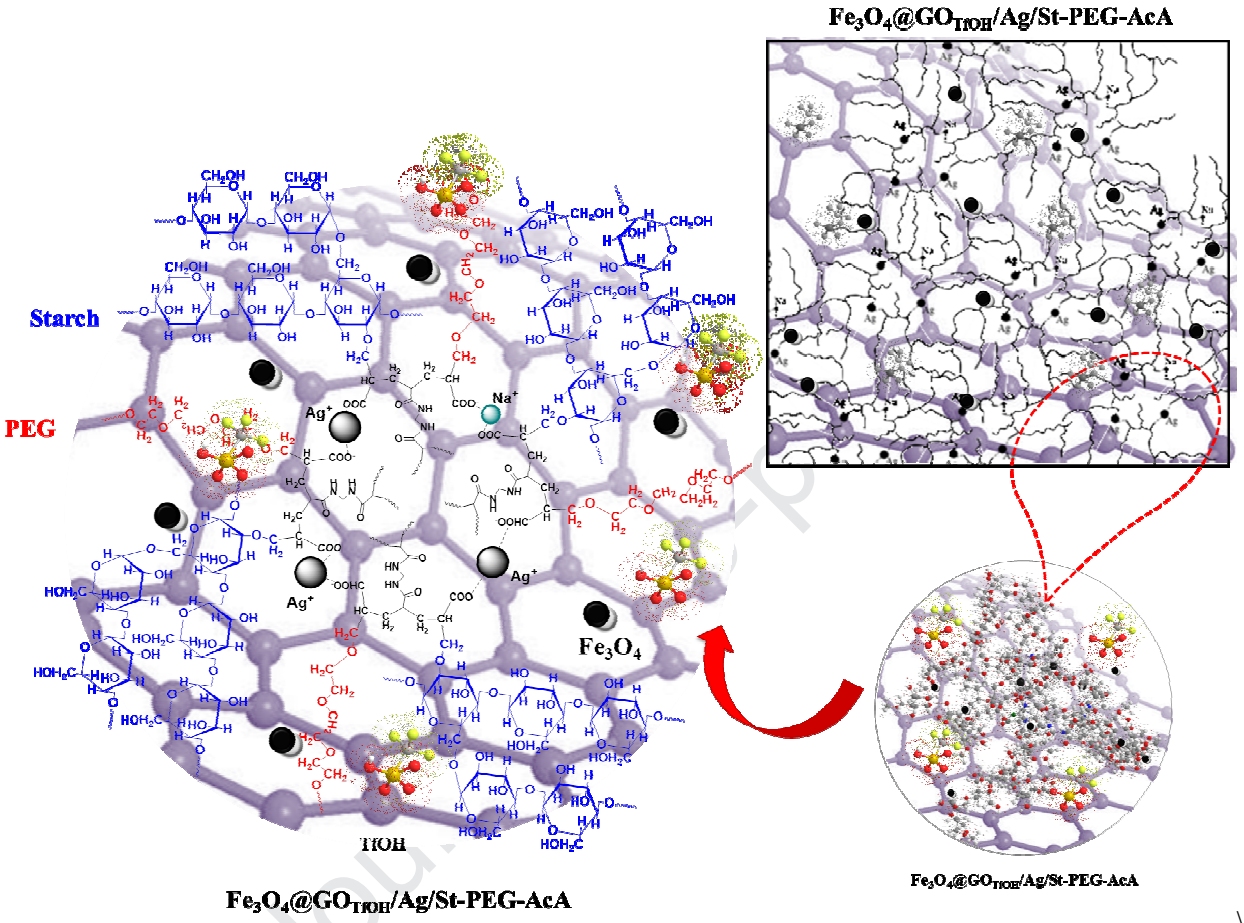

Figure 2: Synthesis of Fe_3O_4@GO_{TfOH}/Ag/St-PEG-AcA

General procedure for the synthesis of 2,4,6-triarylpyridines:

A mixture of an aryl aldehyde (1 mmol), acetophenone (2 mmol), ammonium acetate (1.3 mmol), Fe_3O_4@GO_{TfOH}/Ag/St-PEG-AcA and water (2 mL) was stirred at room temperature for the indicated times (**Scheme 1**). After completion of the reaction, the precipitated solid after magnetically-separation of the catalyst was collected by filtration under suction, washed with cold water, and then recrystallized from n-hexane to afford pure products 1-13 (Table 2) in high yields.

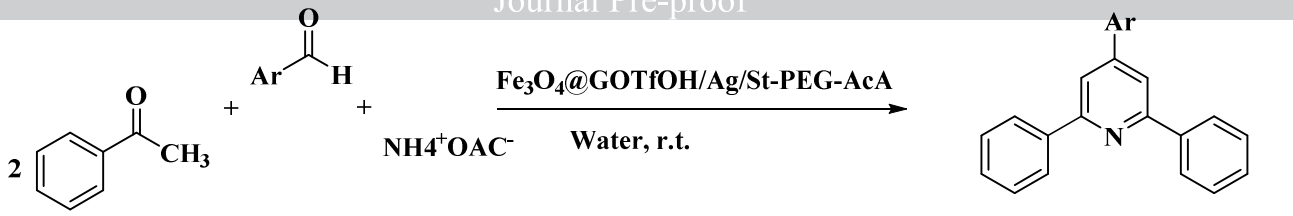

Scheme 1: Synthesis of 2,4,6-triarylpyridines

Characterizations

Melting points were recorded on a Buchi B-540 apparatus. IR spectra were recorded on an ABB Bomem Model FTLA200-100 instrument. ^{1}H and ^{13}CNMR spectra were measured on a Bruker DRX-300 spectrometer, at 300 and 75MHz, using TMS as an internal standard. Chemical shifts (δ) were reported relative to TMS, and coupling constants (J) were reported in hertz (Hz). X-ray powder diffraction (XRD) was carried out on a Philips X'Pertdiffractometer with CoKα radiation. The morphology characteristics of synthesized samples were evaluated using field emission scanning electron microscopy (SEM, Hitachi S-4800). The thermogravimetric analysis (TGA) was measured under a nitrogen atmosphere with a TG/DTA7300 from room temperature to 700°C with a heating rate of 10°C/min. The crystal phases of the samples were analyzed using X-ray diffractometer (XRD, M21X, MAC Science Ltd., Japan) with Cu-Kα radiation. UV-vis diffuse reflectance spectra (DRS) were recorded on a UV-vis spectrophotometer (Cary 300, USA) with an integrating sphere. The chemistry of the surface of nanocatalyst was also determined using X-ray photoelectron spectroscopy (XPS, K-Alpha 1063, Thermo Fisher Scientific, England).

Swelling measurements

A 100 mesh nylon screen, i.e., tea bag containing Fe_3O_4@GO_{TfOH}/Ag/St-PEG-AcA (0.2 ± 0.01 g) with average particle sizes between 40–60 mesh (250–350 mm) was immersed in distilled water or 0.1 M of NaCl solution (100 mL) and allowed to soak for 5 h at room temperature. The teabag was suspended for 10 min to the excess fluid to drain. The equilibrated swelling (ES) was determined in duplicate using the following **Eq. 1**[26]:

$$ES\ (g/g) = \frac{Weight\ of\ swollen\ gel - Weight\ of\ dried\ gel}{Weight\ of\ dried\ gel} \qquad \textbf{Eq. 1}$$

The accuracy of the measurements was ±3%.

Swelling kinetics

In order to measure the absorbency rate of the prepared material, different particle sizes of samples (0.2 ± 0.01 g) were prepared, immersing in 100 mL distilled water using teabags. At pre-determined time intervals, the equilibrium swelling capacity of the materials was evaluated using the above procedure[27].

Antibacterial measurements

The potential of prepared nanocomposite in the field of antibacterial properties was examined using the agar diffusion method against a gram-negative *E. coli.* as a model bacterium. In this method, the bacteria cultures were grown onto nutrient agar plates after sterilized by autoclaving for 1.5 hours at 100 °C. Then, nanocomposite hydrogel (0.1 g) was suspended in distilled water after sonication and loaded onto the above nutrient agar plates. Incubation of the inoculated plates was done at 38 ºC for 38 h, then, the diameters (mm) of the inhibition zones were determined in three directions, and the average was calculated.

In vivo study

Fe_3O_4@GO_{TfOH}/Ag/St-PEG-AcA was tested in vivo for its ability to promote the wound healing process. Ten young C57BL/6NHsd (Charles River) male mice, aged 20–22 months, were selected and separated into two treatment groups of control (5 mice) and Fe_3O_4@GO_{TfOH}/Ag/St-PEG-AcA healed (5 mice). They were kept under standard laboratory conditions in terms of food and water ad libitum. These procedures were approved by the local Ethics Committee for Animal Welfare[28]. The backs of the mice were firmly shaved and subsequently pinched (with the diameter of 12 mm) between two ceramic disc magnets with a thickness of 5 mm, a weight of 2 g, and strength of 3,740 G. Three ischemia-reperfusion (IR) injury cycles were performed. A single cycle consisted of dorsal skin magnet pinch for 12 h followed by a rest period of 12 h. Ulcer formation was diagnosed by an appearance of a disrupted epidermis. The mice were then anesthetized using an intraperitoneal injection of Avertine (tribromoethanol, 250 mg/kg, Sigma, Germany). On the control group, ulcers were wetted with sterile saline and then bandaged with cotton gauze while in Fe_3O_4@GO_{TfOH}/Ag/St-PEG-AcA healed group, ulcers were treated with scaffolds secured in place using 5-0 nylon suture. After 1, 5, 15, and 20 days, the wound size was measured by using a Vernier caliper and a subsequent calculation of wound area (mm^2) using length and width measurements. On day 21 of the experiment when the wound had completely healed, the skin samples were taken for histological study.

Results and Discussion

Figure 3 showed the FTIR spectra of prepared Fe_3O_4@GO_{TfOH}/Ag/St-PEG-AcA compared with Fe_3O_4@GO-TfOH and starch. The FT-IR band of resulted catalyst in the region of 1168 and 680 cm^{-1} is attributed to the stretching vibrations of the (S=O) and (F-O), respectively. The strong-broad peak appeared at about 3340 cm^{-1} is due to the stretching of (O-H) groups in the acidic portion of CF_3SO_3H. The broadband of Fe_3O_4@GO_{TfOH}/Ag/St-PEG-AcA at 3000-3600 cm^{-1} was related to the stretching vibration of OH groups on both starch and PEG polymers. The skeletal mode vibration of the glycoside linkage is illustrated at 900-950 cm^{-1}. The peak around 2962 cm^{-1} and 1472 $cm^{-1}$are related to the CH stretching and bending mode. Meanwhile, in this graph, two other characteristics peaks of carboxylate ion were visible[29]. The first peak is at about 1403 cm^{-1}, assigned to the symmetric stretching mode of the carboxylate ion, while the second peak is at 1580 cm^{-1} due to the asymmetric stretching mode of COO^- groups[30]. These results suggested that the grafted acrylic acid monomers were a presence in two forms of non-ionized (COOH) and ionized (COO^-) onto the polymer backbone[31].

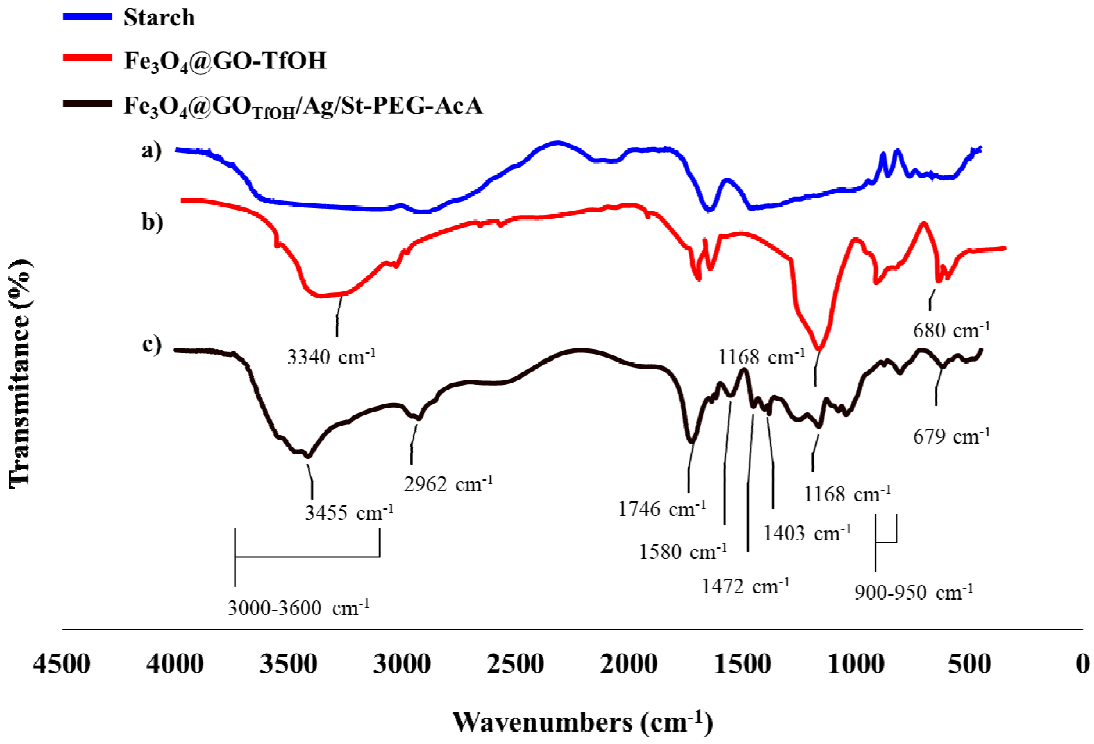

Figure 3: The FT-IR spectra of Fe_3O_4@GO_{TfOH}/Ag/St-PEG-AcA compared to starch and Fe_3O_4@GO-TfOH

Figure 4 shows the UV-vis spectroscopy spectra of Fe_3O_4@GO_{TfOH}/Ag/St-PEG-AcA compared with Fe_3O_4@GO-TfOH and AgNPs. As can be seen, Fe_3O_4@GO-TfOH absorbed below 400 nm in the UV-vis spectrum. However, Ag nanoparticles appeared a single significant peak with a maximum wavelength at about 400 nm, which assigned to the typical surface Plasmon resonance (SPR) of spherical silver nanoparticles. However, in the spectrum of the Ag nanoparticles stabilized by nanocomposite revealed a sharp absorption peak with a slightly shifting in SPR peak value in the range of 400-415 nm with the appearance of a secondary absorbance peak below 400 nm[32]. Based on the above results and the absence of aggregation of Ag nanoparticles in the nanocomposite hydrogel matrix, it is concluded that very stable nanoparticles of Ag were formed and dispersed.

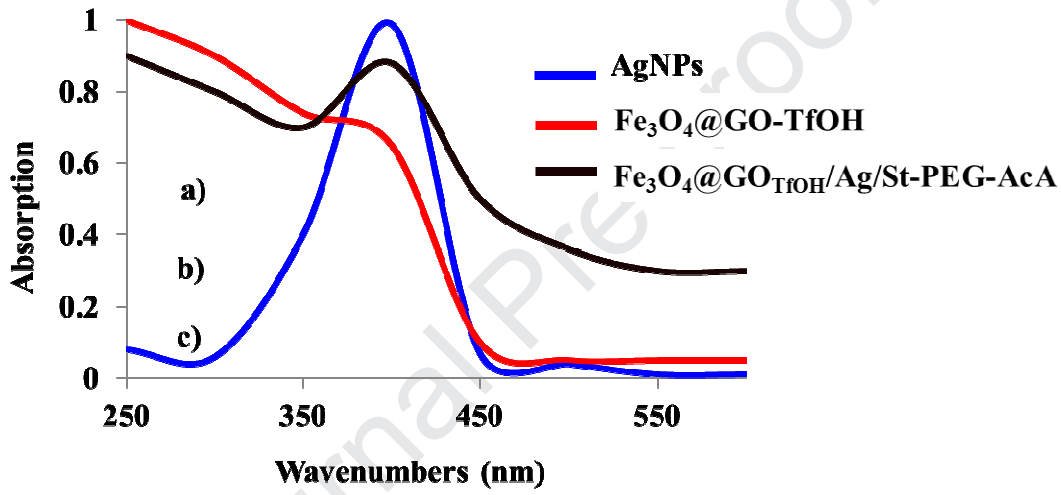

Figure 4: The UV spectra of Fe_3O_4@GO_{TfOH}/Ag/St-PEG-AcA compared to AgNPs and Fe_3O_4@GO-TfOH

SEM, TEM, EDX, and AFM techniques have been used to evaluate the incorporation of AgNPs into the nanocomposite matrix, the morphology, and the topography of prepared material. In **Figure 5a** and **b**, it was clearly indicated that the embedded nanoparticles of Fe_3O_4@GO-TfOH were presented in the range of 83-99 nm with uniform-rough morphology. At the same time, Fe_3O_4@GO_{TfOH}/Ag/St-PEG-AcA had porosity structure. Investigating the interphase characterization, the Ag/St-PEG-AcA hydrogel network placed primarily alongside the surface of Fe_3O_4@GO-TfOH, Fe_3O_4@GO_{TfOH}/Ag/St-PEG-AcA showed a mixed type of growth behavior. This is due to the changing interaction of the hydrogel layer with catalyst surface caused by the difference in surface morphology, texture, composition, and surface area to volume ratio of GO sheets and hydrogel networks [33]. Close inspection of SEM images (Figure 5a and b) exhibits that agglomeration of Fe_3O_4@GO-TfOH and Ag/St-PEG-AcA with the fine state of dispersion.

In **Figure 5c** and **d**, the presence of elements was illustrated in Fe_3O_4@GO_{TfOH}/Ag/St-PEG-AcA. **Figure 5e** showed the elemental composition of nanocatalysts; it was calculated that Fe_3O_4@GO_{TfOH}/Ag/St-PEG-AcA contained about 65.69 % of carbon, 16.86 % of oxygen, 9.68 % of nitrogen, 4.00 % of sulfur, 2.02 % of sodium, 1.00% iron and 0.42 % of silver. The results confirmed the deposition of Ag nanoparticles in the nanocomposite hydrogel matrix.

The morphology, shape, and distribution of AgNPs size were determined by analyzing the TEM images of the nanocomposite hydrogel. The images of TEM were shown in **Figure 6**. It confirmed a highly uniform distribution of the spherical AgNPs with the average of size particles ranges between 20-30 nm inside the nanocomposite hydrogel.

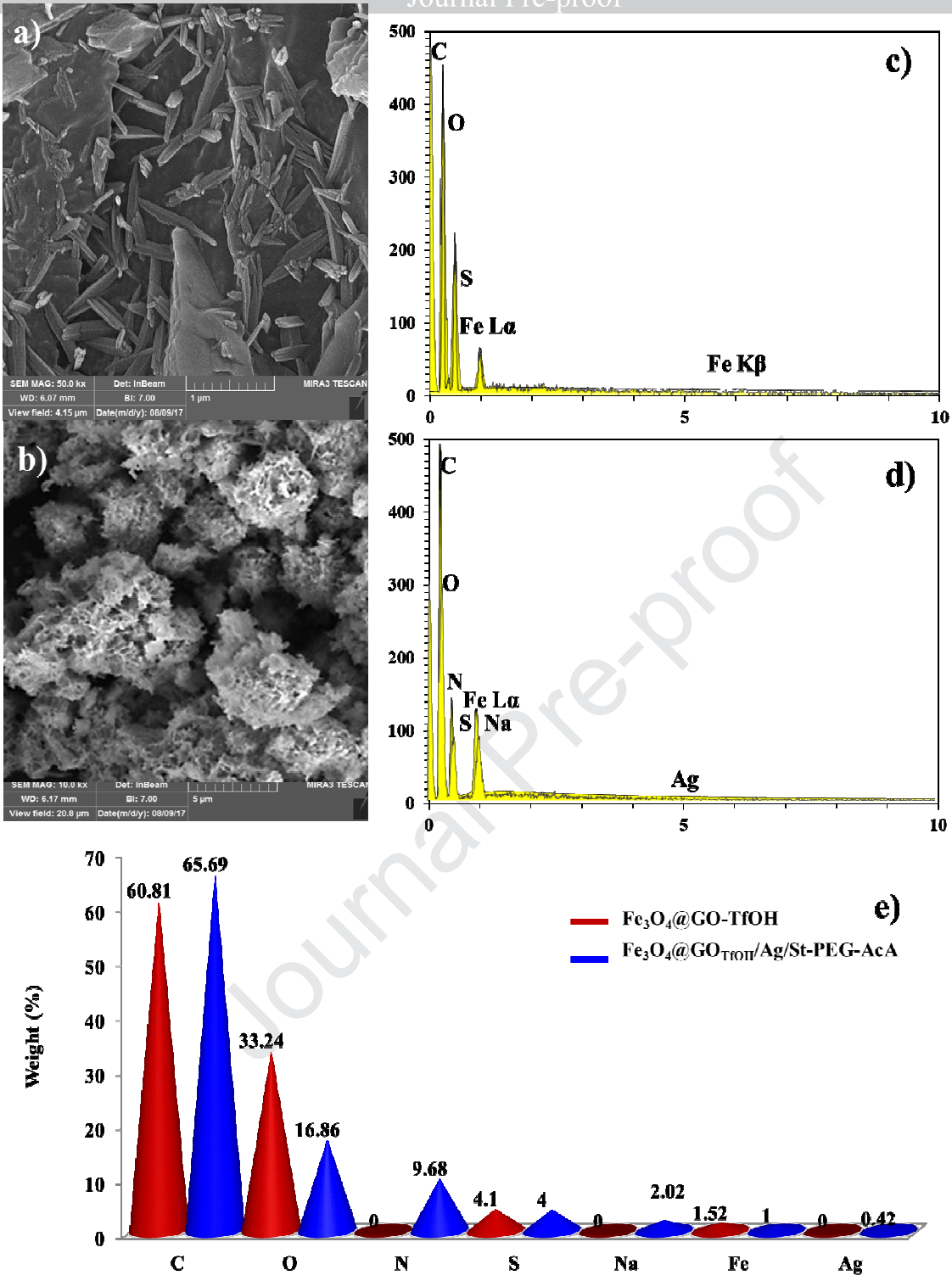

Figure 5: The SEM images, EDX spectra, and the element percentages of Fe_3O_4@GO-TfOH (a, c and d), $Fe_3O_4@GO_{TfOH}$/Ag/St-PEG-AcA (b, d, and d), respectively.

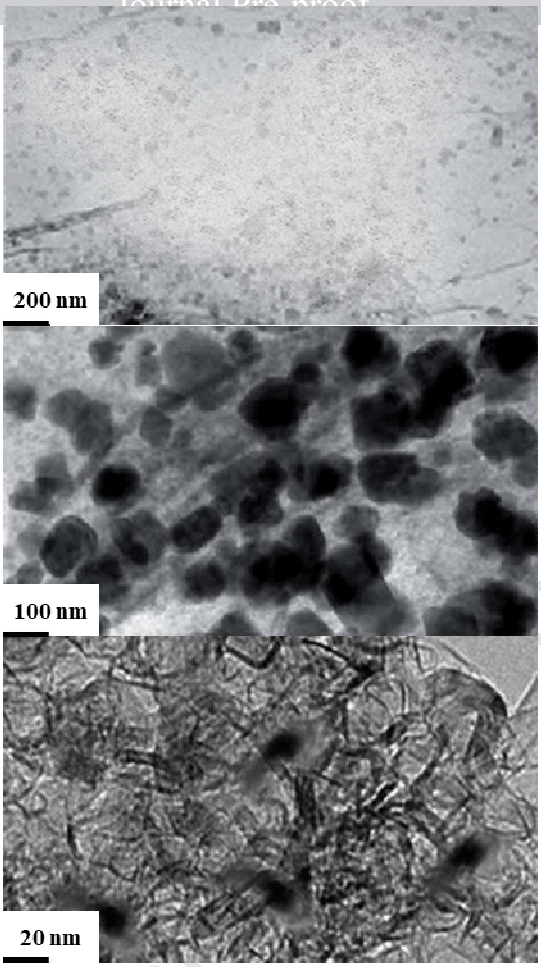

Figure 6: TEM images of Fe_3O_4@GO_{TfOH}/Ag/St-PEG-AcA

In **Figure 7**, AFM images were depicted the surface morphology of the nanocatalysts. Comparing the 2D and 3D images in **Figure 7 a-d**, the surface morphology for Fe_3O_4@GO-TfOH was shown to be a smooth while for Fe_3O_4@GO_{TfOH}/Ag/St-PEG-AcA nanocomposite was a rough surface with clustered features. The histogram in **Figure 7e** plotted the longitudinal section diagram of nanocomposite hydrogel indicated the homogeneous size distribution of Ag nanoparticles with an average size of 45-50 nm.

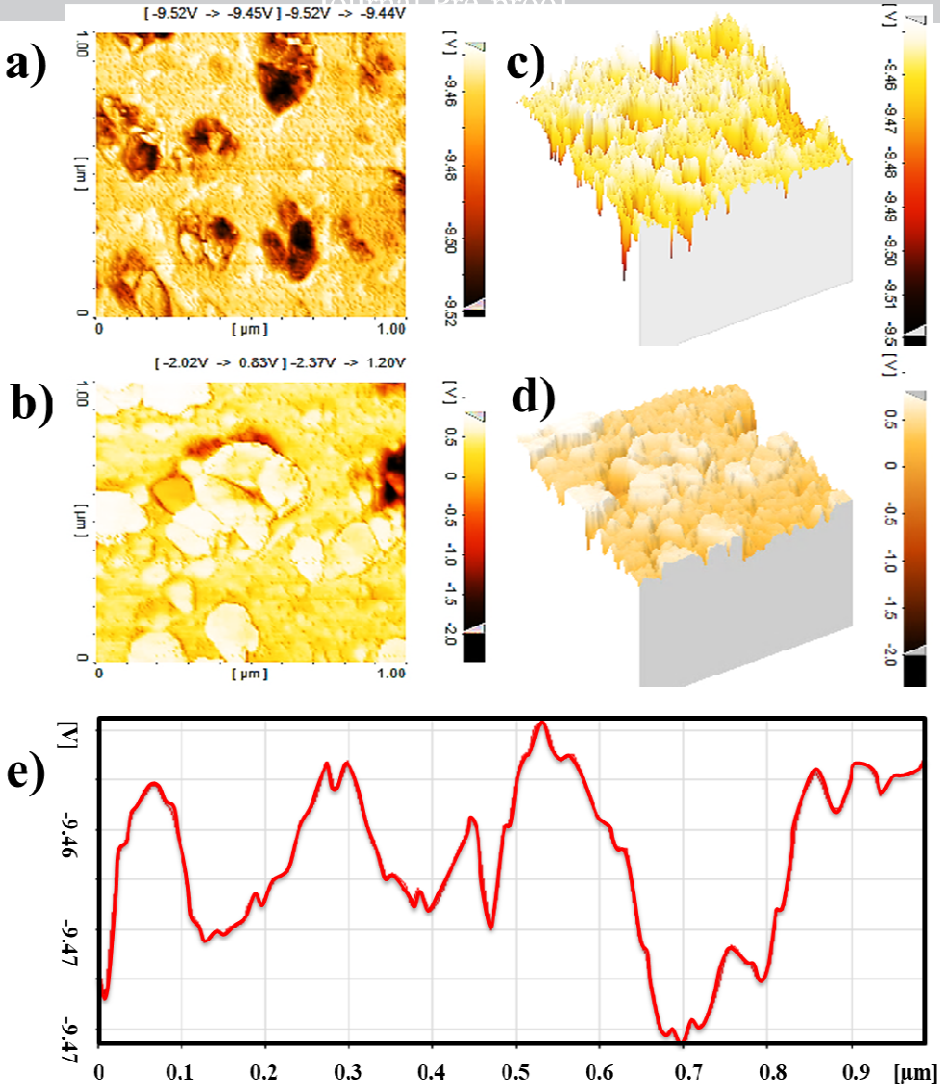

Figure 7: AFM 2D and 3D images of Fe_3O_4@GO_{TfOH}/Ag/St-PEG-AcA (a, b), and Fe_3O_4@GO-TfOH (c, d), respectively and the longitudinal section diagram of Fe_3O_4@GO_{TfOH}/Ag/St-PEG-AcA (e)

Analyzing the structure of Fe_3O_4@GO-TfOH and Fe_3O_4@GO_{TfOH}/Ag/St-PEG-AcA using X-ray diffraction was illustrated in **Figure 8**. As shown in the XRD patterns, Fe_3O_4@GO-TfOH showed a sharp diffraction peak at 34.20°, which originated from the diffraction GO on its (002) layer planes. In general, synthetic nanocatalyst showed diffraction peaks indexed to planes of cubic Fe_3O_4 units including (220), (311), (400), (422) and (511), appearing at 30.11°, 34.20°, 43.80°, 56.03° and 60.99◦, respectively. In contrast, Fe_3O_4@GO_{TfOH}/Ag/St-PEG-AcA exhibited relative sharp peaks at 2θ = 57.1°, 67.2° and 102.34° which were assigned to planes of the silver structure and 2θ = 31.01°, 33.19°, 46.20° and 55.90° which were related to planes of GO and Fe_3O_4 nanoparticles. In addition, the slight difference between XRD patterns of the nanocomposite and AgNPs can be concluded that the AgNPs into nanocomposite matrix were well crystallized. Furthermore, no peaks

related to the impurities were observed in XRD patterns. The average particle size of the trapped AgNPs into the Fe_3O_4@GO_{TfOH}/Ag/St-PEG-AcA Based on the Debye-Scherrer equation was found about 45 nm with the good agreement with the results of AFM and TEM analysis [34].

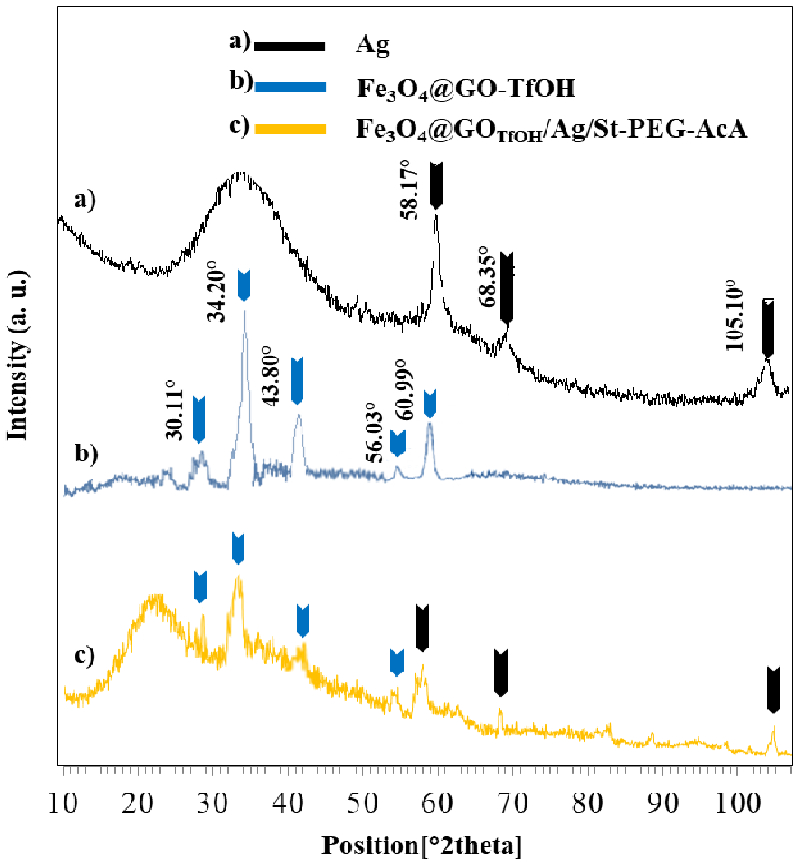

Figure 8: XRD patterns of Ag, Fe_3O_4@GO-TfOH and Fe_3O_4@GO_{TfOH}/Ag/St-PEG-AcA

Figure 9 represented the TGA/DTG analysis of Fe_3O_4@GO-TfOH and Fe_3O_4@GO_{TfOH}/Ag/St-PEG-AcA. Two steps of decomposition were seen for Fe_3O_4@GO-TfOH. The first weight loss at 150-250 °C was due to the evaporation of adsorbed water, and the second rapid weight loss was due to the thermal degradation of the organic content of Fe_3O_4@GO-TfOH structure in the range 400-500 °C (**Figure 9a**). Similar decomposition steps were also seen for Fe_3O_4@GO_{TfOH}/Ag/St-PEG-AcA (**Figure 9b**). Also, the total weight loss of Fe_3O_4@GO_{TfOH}/Ag/St-PEG-AcA and Fe_3O_4@GO-TfOH was about 66 % and 81% at 800 °C, respectively. According to these results and values of nanocomposite compared to Fe_3O_4@GO-TfOH, such as 195.91 °C, which was higher compared to that of the hydrogel, the higher thermal stability of Fe_3O_4@GO_{TfOH}/Ag/St-PEG-AcA was concluded. The presence of silver nanoparticles might be the reason for this high thermal stability in the nanocomposite matrix[35].

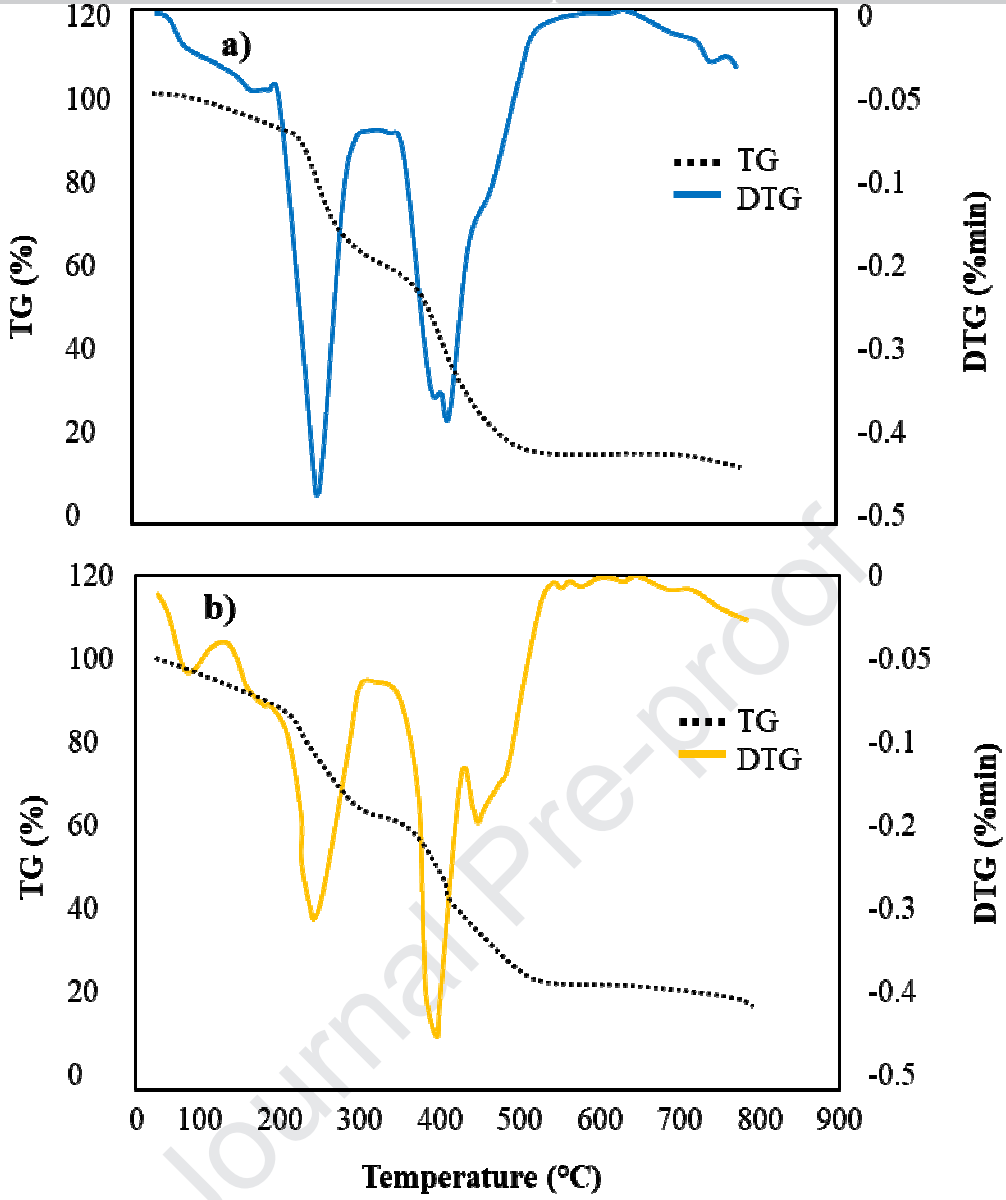

Figure 9: TGA/DTG analysis of Fe_3O_4@GO-TfOH (a) and Fe_3O_4@GO_{TfOH}/Ag/St-PEG-AcA (b)

Swelling characteristics of prepared Fe_3O_4@GO_{TfOH}/Ag/St-PEG-AcA nanocomposite hydrogel are shown in **Figure 10a-e** with 0.1, 0.3, 0.5 and 0.6 mol L^{-1} APS concentration, 0.002, 0.004 and 0.006 mol L^{-1} MBA concentration, 0.5 and 1.2 mol L^{-1} AcA concentration, 0.75 and 1.5 wt% PEG concentration, 100, 200, 400, 600 and 800 ppm AgNPs. All of these swelling experiments were carried out at a pH of 7 in water. Swelling ratios of samples synthesized with optimized reaction parameters are also shown in **Figure 10f** at pH 6.5, 7, and 8.5. In **Figure 10a**, it is observed that increasing the concentration of APS from 0.1 to 0.3 mol L^{-1} leads to higher swelling ratios, which may be attributed to the decrease of hydrogel molecular weight due to more chain ends and imperfection of gel network. In the present work, optimum APS concentration was found to be 0.3

mol L^{-1}. Similar trends for the swelling ratio of the hydrogels are also observed for increasing MBA, AcA, and PEG concentrations (**Figure 10b-d**). This may be ascribed to lower crosslinking, higher reactivity, and increased hydrophilicity of the hydrogels, respectively. From **Figure 10e**, it is obvious that increasing the concentration of AgNPs from 100 to 400 ppm, leads to higher swelling ratios which may be related to the capability of AgNPs embedded in the hydrogel to increase the pores and free spaces within the structure of the network of the prepared hydrogel and as a consequence adsorbs more water. Thus, the water absorption properties of the hydrogel improve. However, further increase of silver concentration leads to decreased swelling properties due to filling up the void spaces of the network chains and chelation with some -OH and -C=O groups of Fe_3O_4@GO_{TfOH}/Ag/St-PEG-AcA while neutralizing the repulsions in the networks. Based on the swelling kinetics curves, Fe_3O_4@GO_{TfOH}/Ag/St-PEG-AcA present higher and faster swelling ratios compared to the corresponding pure hydrogel. This may be attributed to the presence of AgNPs within the surface charges of the gel network and the presence of different sizes of AgNPs in an efflux of water to balance the build-up of ion osmotic pressure.

From **Figure 10f**, it is observed that at higher pH swelling ratio increases, which may be due to ionization of hydrophilic -COOH groups of the hydrogels. The swelling data of the hydrogels including ESR, the initial rate of swelling (r_i), rate constant (k_{rs}) and statistical parameters such as R^2, χ^2 , F of the kinetic fittings confirmed close fitting of the swelling data to second-order rate equation due to regression coefficient R^2 (0.97-0.99) of these fittings are close to unity. At the same time, chi-square χ^2 (0.007-0.2) of these fittings are very low and F values are very high (900-4400) and also calculated ES ratio of pure hydrogel (11.9) and Fe_3O_4@GO_{TfOH}/Ag/St-PEG-AcA (13.1) was also very close to their experimental ES ratios as shown in **Figure 10f**.

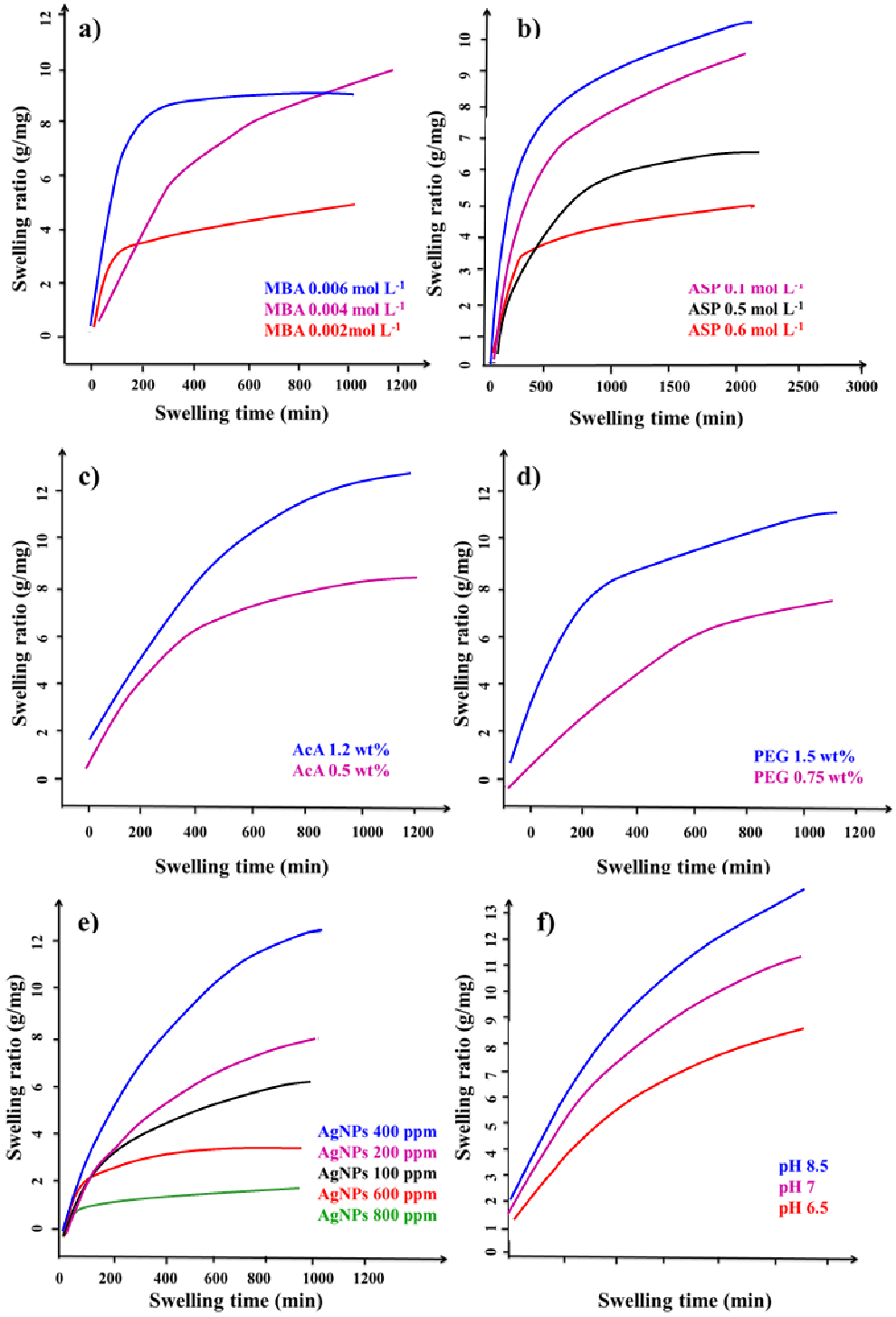

Figure 10: Swelling characteristics of prepared Fe_3O_4@GO_{TfOH}/Ag/St-PEG-AcA nanocomposite hydrogel under the effect of a) crosslinker (MBA), b) initiator concentration (APS), c) AcA monomer concentration, d) PEG monomer concentration, e) AgNPs solution concentration and f) pH on swelling ration data

The antimicrobial effect (*in vitro*) of prepared materials was investigated by comparing the diameter of the growth inhibition zones of *E. coli.* As can be seen from **Figure 11**, both

Fe_3O_4@GO_{TfOH}/Ag/St-PEG-AcA and Fe_3O_4@GO-TfOH showed the antibacterial effect on the bacteria, *E. coli*, after 24 h of incubation at 37 °C. So that, paper discs soaked for Fe_3O_4@GO-TfOH with two different concentrations exhibited inhibition zone values of 3.83 mm (for 1.5 mg L^{-1}) and 5.70 mm (for 3 mg L^{-1}) against *E. coli*. Similarly, according to Fig. 14, Fe_3O_4@GO_{TfOH}/Ag/St-PEG-AcA exhibited inhibition zone values of 10.56 mm (for 1.5 mg L^{-1}), and 13.32 mm (for 3 mg L^{-1}) against *E. coli* with the same concentrations. In this study, the results obtained that the Fe_3O_4@GO_{TfOH}/Ag/St-PEG-AcA showed further potential antibacterial activity than the Fe_3O_4@GO-TfOH under similar test conditions. This could be related to the presence of AgNPs and the presence of a more porous structure of nanocomposite hydrogel, which during the swelling process, released the silver nanoparticles efficiently into the media and led to its interaction with the lipid layer of the bacterial cell membrane[36]. Since gram-negative *E. coli* has a thin lipid layer of the cell wall may lead to a facilitate penetration of released silver nanoparticles into the bacterial cell membrane[37]. The released AgNPs can then destroy with the lipid layer of the cell membrane.

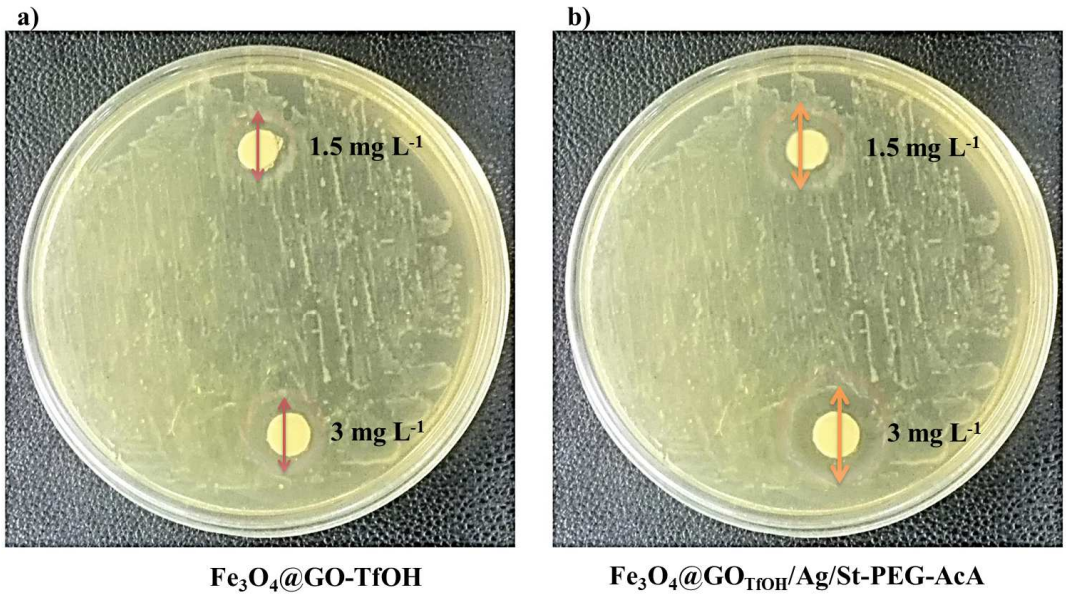

Figure 11: Antimicrobial effect (*in vitro*) of Fe_3O_4@GO_{TfOH}/Ag/St-PEG-AcA and Fe_3O_4@GO-TfOH

The in vivo model of ulceration was performed as described in the experimental section. Ulceration was induced by magnet pressure. In treated animals, the epidermis showed visible signs of ulceration at least 3 days after the last cycle of magnet treatment. A significant reduction of the area of lesion was observed following treatment of animals with Fe_3O_4@GO_{TfOH}/Ag/St-PEG-AcA H at

5 and 15 days when compared with the control group (**Figure 12a**). It is interesting to observe that the Fe_3O_4@GO_{TfOH}/Ag/St-PEG-AcA treatment significantly increased the wound closure at 15 days compared with the treatment at 5 days. Furthermore, the results also showed the signs that the wounds treated and covered with the samples of Fe_3O_4@GO_{TfOH}/Ag/St-PEG-AcA healed very faster than wounds treated with the control group (**Figure 12b**). The expressively expedited wound healing can also be perceived in the Fe_3O_4@GO_{TfOH}/Ag/St-PEG-AcA-treated wounds at day 15.

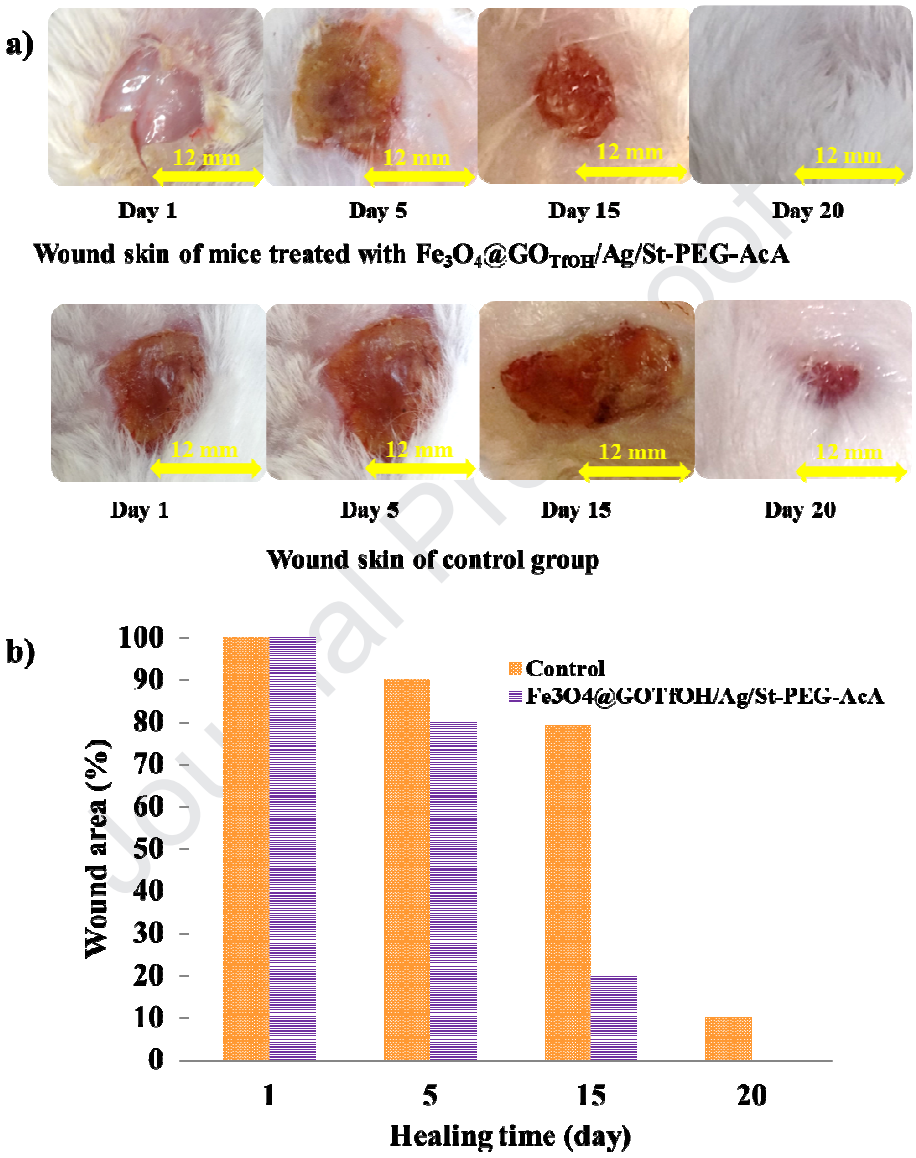

Figure 12: The in vivo model of ulceration

Figure 13 shows the skin histology on day 21. The Fe_3O_4@GO_{TfOH}/Ag/St-PEG-AcA healed group showed complete healing, as indicated by the uniformly packed parallel collagen fibers. These suggest that the beginning of the macromolecular organization of the granulation tissue. For control wounds, the tissue contained large numbers of fibroblasts, which were irregularly arranged, and

there was a less compact arrangement of collagen fibers compared to Fe_3O_4@GO_{TfOH}/Ag/St-PEG-AcA healed wounds. The dermis of mice treated with Fe_3O_4@GO_{TfOH}/Ag/St-PEG-AcA showed similar fibroblast and fibrillar arrangement of the control wounds.

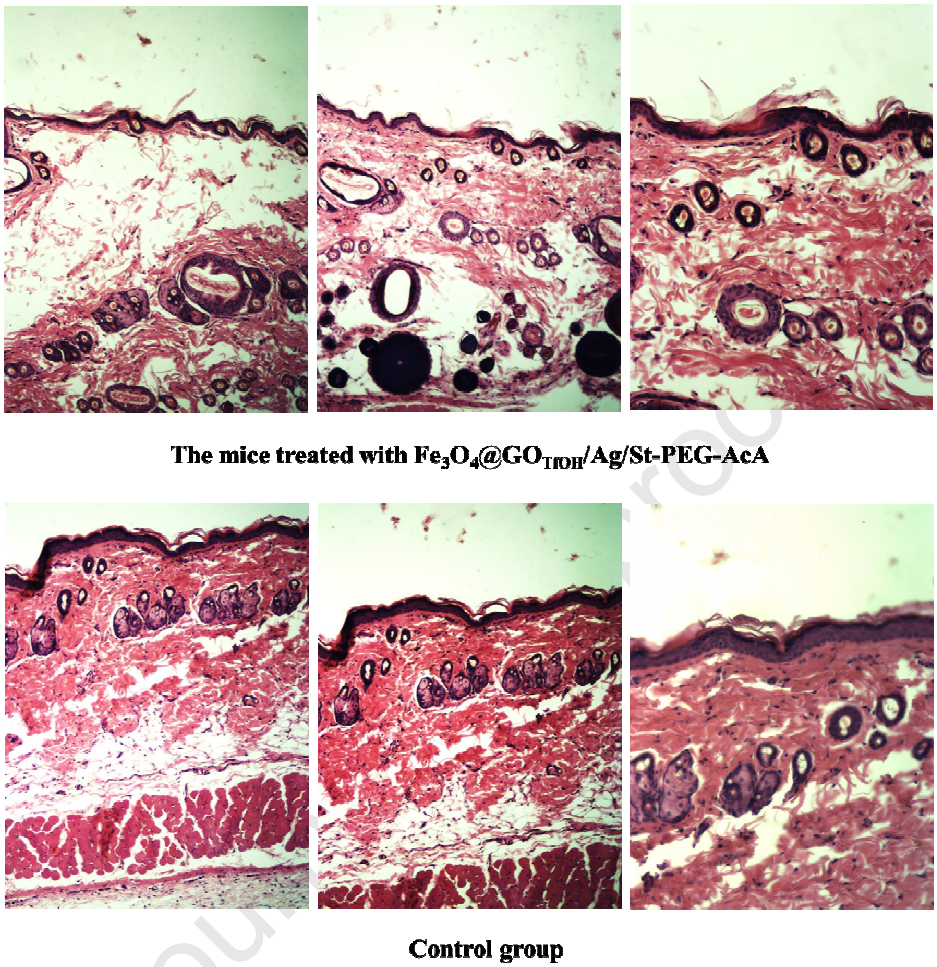

Figure 13: The skin histology on day 21

With the increasing demand in modern organic synthesis for more pure compounds, we decided to deliberate the efficiency of Fe_3O_4@GO_{TfOH}/Ag/St-PEG-AcA as a novel magnetic catalyst in the synthesis of 2,4,6-triarylpyridines in water. The reaction between acetophenone, 4-chlorobenzaldehyde, and ammonium acetate in water solvent system was selected as a model (**Scheme 2**). Increasing the reaction temperature and amount of the catalyst up to room temperature and 0.03 g, respectively, increased the yield of products, whereas the further increase in both temperature and amount of catalyst was met not to affect the formation of the products. On the other hand, very low catalytic activity is observed for varied organic solvents such as EtOH, MeOH, MeCN, and $CHCl_3$, under reflux condition and in the presence of 0.03 g of Fe_3O_4@GO_{TfOH}/Ag/St-PEG-AcA (**Table 1**).

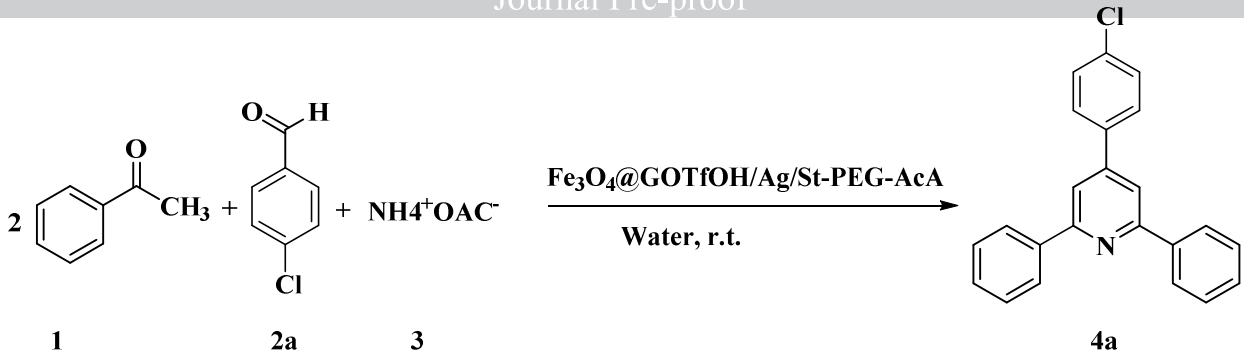

Scheme 2: The model reaction between acetophenone, 4-chlorobenzaldehyde, and ammonium acetate in water in the presence of $Fe_3O_4@GO_{TfOH}$/Ag/St-PEG-AcA

Table 1: Optimizing the condition of the model reaction

Entry	Catalyst (g)	Solvent	Temperature (^oC)	Time (min)	Yield[a] (%)
1	-	-	120	300	Trace
2	0.01	-	r.t.	60	50
3	0.01	H_2O	r.t.	10	88
4	**0.03**	**H_2O**	**r.t.**	**6**	**94**
5	0.05	H_2O	r.t.	6	94
6	0.03	H_2O	80	6	94
7	0.03	EtOH	reflux	60	60
8	0.03	MeOH	reflux	60	66
9	0.03	MeCN	reflux	60	68
10	0.03	$CHCl_3$	reflux	60	70

[a]Isolated yields

All the reaction with substituted benzaldehydes preceded very cleanly at optimized reaction conditions, and no undesirable side-reaction were observed, although the yields were dependent on the substituent. To check the versatility of this method, we had also studied the various hetero arylaldehydes summarized in **Table 2**.

For demonstrating the matchless catalytic behavior of $Fe_3O_4@GO_{TfOH}$/Ag/St-PEG-AcA and considering the differences between its activity with other catalysts, the comparison of the model reaction system was performed in **Table 3** between $Fe_3O_4@GO_{TfOH}$/Ag/St-PEG-AcA and other reported catalysts[38-44]. It was determined that $Fe_3O_4@GO_{TfOH}$/Ag/St-PEG-AcA is the most effective catalyst for this purpose due to the high surface area and very strong acidity of $-SO_3H$ groups.

Table 2: The reaction time (min) and the yield (%) of 2,4,6-triarylpyridines

Entry	Product	Ar	Time (min)	Yield* (%)
1	4a	4-Cl-Ph	6	97
2	4b	Ph	9	98
3	4c	4-Br-Ph	6	87
4	4d	4-F-Ph	6	83
5	4e	4-Me-Ph	11	78
6	4f	4-OMe-Ph	12	77
7	4g	4-CN-Ph	10	87
8	4h	4-NO_2-Ph	5	90
9	4i	3-NO_2-Ph	7	93
10	4j	3,4-diCl-Ph	5	86
11	4k	4-OH-Ph	10	92
12	4l	naphthalen-1-yl	5	97
13	4m	thiophen-2-y	5	94

Table 3: Comparison of model reaction system between Fe_3O_4@GO_{TfOH}/Ag/St-PEG-AcA and other reported catalysts

Entry	Catalyst	Time (min)	Temperature (^oC)	Yield* (%)
1	PEG-DAILs[a], 10% mol	45	110	95 [38]
2	Activated Fuller's earth	90	110	90 [39]
3	Fe_3O_4@TiO_2@$O_2PO_2(CH_2)_2NHSO_3H$	20	120	80 [40]
4	-	480	150	97 [41]
5	HNTf2[b], 1% mol	50	80	93 [42]
6	LPSF[c], 0.01 g	60	60	94 [43]
7	ChVO, 5 mg	60	130	80 [44]
8	**Fe_3O_4@GO_{TfOH}/Ag/St-PEG-AcA**	**6**	**r.t.**	**This work**

[a] poly(ethylene glycol)–linked dicationic acidic ionic liquids
[b] triflimide
[c] Fe_3O_4\SiO_2\propyltriethoxysilane\L-proline
[d] chitosan supported vanadium-oxo

The conceivable mechanism is shown in **Figure 14**. On the high surface area of magnetic nanocatalyst, the reactants are easily absorbed. Because of intrinsic Brönsted acidity of -SO_3H and Lewis acidity of the Fe^{3+}, the carbonyl moiety of acetophenone is activated.

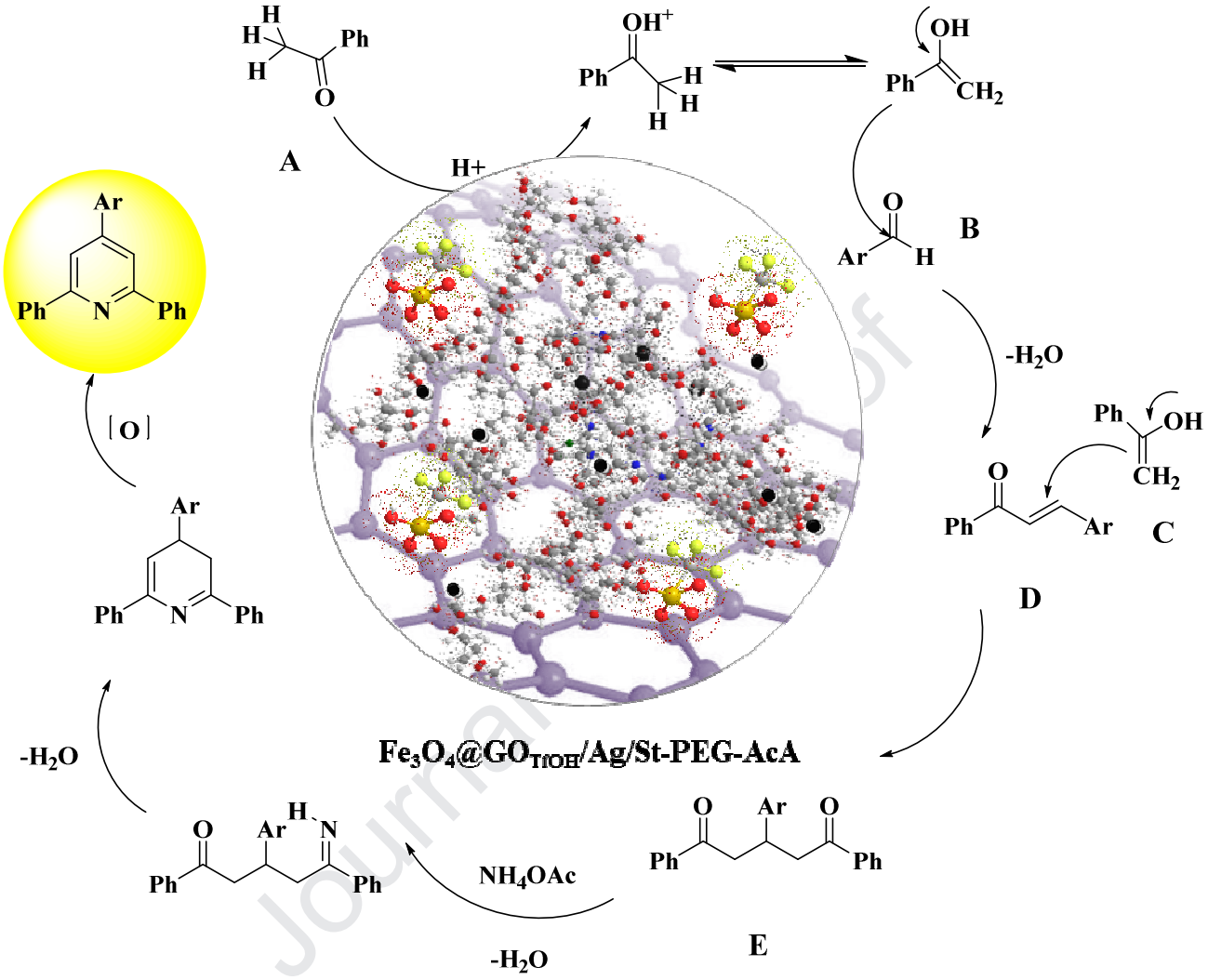

Figure 14: Proposed mechanism for the synthesis of 2,4,6-triarylpyridines in the presence of Fe_3O_4@GO_{TfOH}/Ag/St-PEG-AcA

Anyway, this catalyst can be removed in the presence of an external magnet and be recovered in subsequent runs with the low observation of a significant decrease in activity after 10 runs (**Figure 15**).

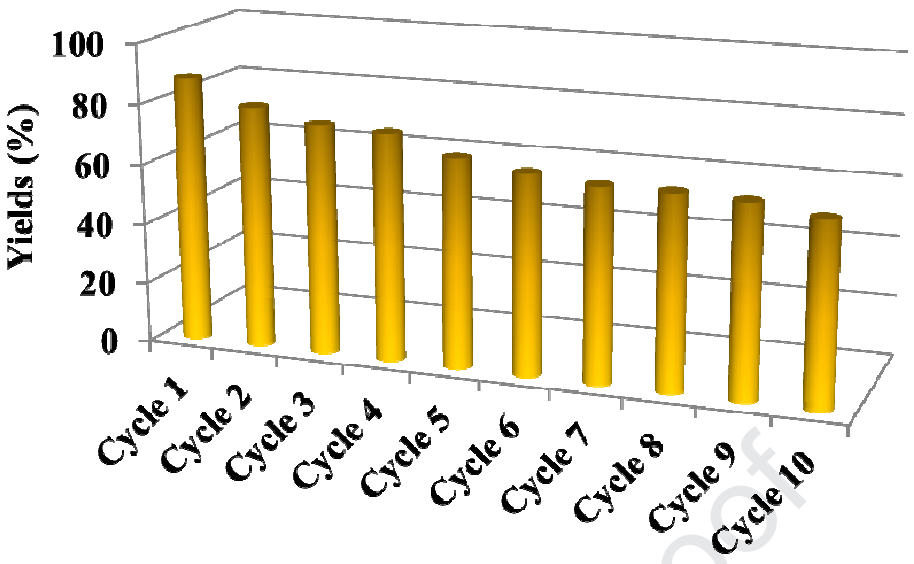

Figure 15: Recovery of catalyst in ten runs

Conclusions

In summary, our new idea that has been done in this project is leading to prepare Fe_3O_4@GO_{TfOH}/Ag/St-PEG-AcA as a magnetically recoverable nanocatalyst for one-pot synthesis of 2,4,6-triarylpyridine derivatives under water solvent by functionalizing (Fe_3O_4)-GO with Trifluoromethanesulfonic acid and combining with hydrogel network of Ag/St-PEG-AcA. This catalyst with better activities to other commercially available sulfonic acid catalysts has made the reaction condition distinctly superior over to many different protocols reported earlier. The prepared nanocatalyst exhibits excellent antimicrobial efficiency toward *E. coli* bacteria. Besides, histology of repaired wounds in Fe_3O_4@GO_{TfOH}/Ag/St-PEG-AcA healed a group of mice showed better fibroblast distribution and more compact collagen fiber organization compared to wounds in the control group.

Acknowledgment

We gratefully thank the Department of chemistry, Institute of Science and Research (SIPTC), Tehran, Iran (www.siptc.ir) for applying the research facilities.

References

[1] Price, Neil PJ, et al. "Rhodium-catalyzed reductive modification of pyrimidine nucleosides, nucleotide phosphates, and sugar nucleotides." *Carbohydrate Research* 488 (2020): 107893.

[2] Pettit, Robert E. "Organic matter, humus, humate, humic acid, fulvic acid and humin: their importance in soil fertility and plant health." *CTI Research* (2004): 1-17.

[3] Kerru, Nagaraju, et al. "Recent advances in heterogeneous catalysts for the synthesis of imidazole derivatives." *Synthetic Communications* 49.19 (2019): 2437-2459.

[4] Sharma, Mamta, Pooja Yadav, and Minakshi Sharma. "Novel electrochemical sensing of galactose using GalOxNPs/CHIT modified pencil graphite electrode." *Carbohydrate research* 483 (2019): 107749.

[5] Shan, Cong, et al. "Graphene oxide enhanced polyacrylamide-alginate aerogels catalysts." *Carbohydrate polymers* 203 (2019): 19-25.

[6] Yao, Mingjun, et al. "Preparation of dialdehyde cellulose graftead graphene oxide composite and its adsorption behavior for heavy metals from aqueous solution." *Carbohydrate polymers* 212 (2019): 345-351.

[7] Ramesh, Sivalingam, et al. "Fabrication of manganese oxide@ nitrogen doped graphene oxide/polypyrrole (MnO2@ NGO/PPy) hybrid composite electrodes for energy storage devices." *Journal of Materials Research and Technology* 8.5 (2019): 4227-4238.

[8] Chyan, Yieu, et al. "Graphene Art." *ACS Applied Nano Materials* 2.5 (2019): 3007-3011.

[9] Xu, Huan, et al. "Thermostable and impermeable “nano-barrier walls” constructed by poly (lactic acid) stereocomplex crystal decorated graphene oxide nanosheets." *Macromolecules* 48.7 (2015): 2127-2137.

[10] Xu, Huan, et al. "Zero-dimensional and highly oxygenated graphene oxide for multifunctional poly (lactic acid) bionanocomposites." *ACS Sustainable chemistry & engineering* 4.10 (2016): 5618-5631.

[11] Çakir, Mustafa, and Emre Akin. "Wear, thermal, and physical properties of fluorine□containing polyimide/silica hybrid nanocomposite coatings." *Journal of Applied Polymer Science* 136.16 (2019): 47399.

[12] Prasanna, SRV Siva, et al. "Metal oxide based nanomaterials and their polymer nanocomposites." *Nanomaterials and Polymer Nanocomposites*. Elsevier, 2019. 123-144.

[13] Sethi, Sapna, B. S. Kaith, and Vaneet Kumar. "Fabrication and characterization of microwave assisted carboxymethyl cellulose-gelatin silver nanoparticles imbibed hydrogel: Its evaluation as dye degradation." *Reactive and Functional Polymers* 142 (2019): 134-146.

[14] Pereira, Anna Karla dos S., et al. "Antibacterial effects and ibuprofen release potential using chitosan microspheres loaded with silver nanoparticles." *Carbohydrate Research* (2019): 107891.

[15] Farzinfar, Elnaz, and Azin Paydayesh. "Investigation of polyvinyl alcohol nanocomposite hydrogels containing chitosan nanoparticles as wound dressing." *International Journal of Polymeric Materials and Polymeric Biomaterials* 68.11 (2019): 628-638.

[16] Dhiman, Navneet K., Shekhar Agnihotri, and Ravi Shukla. "Silver-based polymeric nanocomposites as antimicrobial coatings for biomedical applications." *Nanotechnology in Modern Animal Biotechnology*. Springer, Singapore, 2019. 115-171.

[17] Bianchera, Annalisa, et al. "The Place of Biomaterials in Wound Healing." *Therapeutic Dressings and Wound Healing Applications* (2020): 337-366.

[18] Masood, Nosheen, et al. "Silver nanoparticle impregnated chitosan-PEG hydrogel enhances wound healing in diabetes induced rabbits." *International journal of pharmaceutics* 559 (2019): 23-36.

[19] Rasool, Atta, Sadia Ata, and Atif Islam. "Stimuli responsive biopolymer (chitosan) based blend hydrogels for wound healing application." *Carbohydrate polymers* 203 (2019): 423-429.

[20] Taylor, Alexandria P., et al. "Modern advances in heterocyclic chemistry in drug discovery." *Organic & biomolecular chemistry* 14.28 (2016): 6611-6637.

[21] Smith, Nicole M., et al. "PEG mediated synthesis of amino-functionalised 2, 4, 6-triarylpyridines." *Green Chemistry* 9.11 (2007): 1185-1190.

[22] Qing, Xushun, et al. "One-pot synthesis of 2, 4, 6-triarylpyridines from β-nitrostyrenes, substituted salicylic aldehydes and ammonium acetate." *RSC advances* 6.98 (2016): 95957-95964.

[23] Forouzandehdel, Shayan, Sherwin Forouzandehdel, and Mina Rezghi Rami. "Synthesis of a novel magnetic starch-alginic acid-based biomaterial for drug delivery." *Carbohydrate Research* 487 (2020): 107889.

[24] Rostamizadeh, Shahnaz, et al. "Magnetic Graphene Oxide Anchored Sulfonic Acid as a Novel Nanocatalyst for the Synthesis of N□aryl□2□amino□1, 6□naphthyridines." *Journal of the Chinese Chemical Society* 60.11 (2013).

[25] Shahriary, Leila, and Anjali A. Athawale. "Graphene oxide synthesized by using modified hummers approach." *Int. J. Renew. Energy Environ. Eng* 2.01 (2014): 58-63.

[26] Omidian, Hussein, et al. "Swelling and crosslink density measurements for hydrogels." *Iranian J. of Polymer Science and Technology Vol* 3.2 (1994).

[27] Schott, Hans. "Swelling kinetics of polymers." *Journal of Macromolecular Science, Part B: Physics* 31.1 (1992): 1-9.

[28] Osborne, Nicola J., Daisy Payne, and Michael L. Newman. "Journal editorial policies, animal welfare, and the 3Rs." *The American Journal of Bioethics* 9.12 (2009): 55-59.

[29] Ahmed, Enas M., et al. "Synthesis and swelling characterization of carboxymethyl cellulose-g-Poly (Acrylic acid-co–Acrylamide) hydrogel and their application in agricultural field." *Int. J. ChemTech Res* 9 (2016): 270-81.

[30] Gharekhani, Hamed, et al. "Superabsorbent hydrogel made of NaAlg-g-poly (AA-co-AAm) and rice husk ash: Synthesis, characterization, and swelling kinetic studies." *Carbohydrate polymers* 168 (2017): 1-13.

[31] Kyrychenko, Alexander, et al. "Stimuli-responsive adsorption of poly (acrylic acid) onto silver nanoparticles: Role of polymer chain length and degree of ionization." *Journal of Molecular Liquids* 276 (2019): 243-254.

[32] Basu, Shibani, Himadri Sekhar Samanta, and Jhuma Ganguly. "Green synthesis and swelling behavior of Ag-nanocomposite semi-IPN hydrogels and their drug delivery using Dolichos biflorus Linn." *Soft Materials* 16.1 (2018): 7-19.

[33] Bedi, Harpreet S., Mayank Tiwari, and Prabhat K. Agnihotri. "Quantitative determination of size and properties of interphases in carbon nanotube-based multiscale composites." *Carbon* 132 (2018): 181-190.

[34] Holzwarth, Uwe, and Neil Gibson. "The Scherrer equation versus the'Debye-Scherrer equation'." *Nature nanotechnology* 6.9 (2011): 534-534.

[35] Sun, Junming, et al. "Toward monodispersed silver nanoparticles with unusual thermal stability." *Journal of the American Chemical Society* 128.49 (2006): 15756-15764.

[36] Ahmed, Bilal, et al. "ROS mediated destruction of cell membrane, growth and biofilms of human bacterial pathogens by stable metallic AgNPs functionalized from bell pepper extract and quercetin." *Advanced Powder Technology* 29.7 (2018): 1601-1616.

[37] Yin, Jun, et al. "Attachment of silver nanoparticles (AgNPs) onto thin-film composite (TFC) membranes through covalent bonding to reduce membrane biofouling." *Journal of membrane science* 441 (2013): 73-82.

[38] Ren, Yi-Ming, Ze Zhang, and Shuo Jin. "Convenient and efficient method for synthesis of 2, 4, 6-triarylpyridines using catalytic amount of PEG1000-based dicationic acidic ionic liquid under solvent-free conditions." *Synthetic Communications* 46.6 (2016): 528-535.

[39] Rekunge, Deelip S., Ishwari A. Kale, and Ganesh U. Chaturbhuj. "An efficient, green solvent-free protocol for the synthesis of 2, 4, 6-triarylpyridines using reusable

heterogeneous activated Fuller's earth catalyst." *Journal of the Iranian Chemical Society* 15.11 (2018): 2455-2462.

[40] Zolfigol, Mohammad Ali, et al. "Catalytic application of sulfonic acid□functionalized titana□coated magnetic nanoparticles for the preparation of 1, 8□dioxodecahydroacridines and 2, 4, 6□triarylpyridines via anomeric□based oxidation." *Applied Organometallic Chemistry* 32.2 (2018): e4063.

[41] Adib, Mehdi, Neda Ayashi, and Peiman Mirzaei. "An Efficient Synthesis of 2, 4, 6-Triarylpyridines by Use of Benzyl Halides under Neat Conditions." *Synlett* 27.03 (2016): 417-421.

[42] Wang, Hongshe, et al. "An efficient one pot three-component synthesis of 2, 4, 6-triarylpyridines using triflimide as a metal-free catalyst under solvent-free conditions." *RSC advances* 9.9 (2019): 5158-5163.

[43] Maleki, Ali, and Razieh Firouzi-Haji. "L-Proline functionalized magnetic nanoparticles: A novel magnetically reusable nanocatalyst for one-pot synthesis of 2, 4, 6-triarylpyridines." *Scientific reports* 8.1 (2018): 1-8.

[44] Safaiee, Maliheh, et al. "Synthesis and application of chitosan supported vanadium oxo in the synthesis of 1, 4-dihydropyridines and 2, 4, 6-triarylpyridines via anomeric based oxidation." *New Journal of Chemistry* 42.15 (2018): 12539-12548.

Design and application of (Fe_3O_4)-GO_{TfOH} based AgNPs doped Starch/PEG-poly (acrylic acid) nanocomposite as the magnetic nanocatalyst and the wound dress

Shayan Forouzandehdel[a], Maryam Meskini[b], Mina Rezghi Rami[c]*

[a] Department of Chemistry, Sharif University of Technology, P. O. Box 11365-9516, Tehran, Iran
[b] Microbiology Research Center (MRC), Pasteur Institute of Iran, Tehran, Iran
[c] Department of Chemistry, K. N. Toosi University of Technology, P. O. Box 15875-4416, Tehran, Iran.

*rezghi@siptc.ir

Highlights:

1) Synthesis of nanocomposite hydrogel network (Fe_3O_4)-GO_{TfOH} based Ag nanoparticles doped Starch/PEG-poly (acrylic acid) nanocomposite

2) one-pot synthesis of 2,4,6-triarylpyridine derivatives in water

3) Excellent biocompatibility of the prepared nanocomposite for wound healing

4) Good antimicrobial efficiency of the nanocomposite toward *E. coli* bacteria

5) Fine fibroblast distribution and good compact collagen fiber for wounds headed with the nanocomposite

Declaration of interests

☒ The authors declare that they have no known competing financial interests or personal relationships that could have appeared to influence the work reported in this paper.

☐The authors declare the following financial interests/personal relationships which may be considered as potential competing interests:

Mina Rezghi Rami
Shayan Forouzandehdel
Maryam Meskini